Eddy Current Modelling for Inspection of Riveted Structures in Aeronautics

S. Paillard †, G. Pichenot †, M. Lambert ‡, H. Voillaume +
† *: CEA/LIST, CEA Saclay 91191 Gif-sur-Yvette France.*
‡ *: L2S (CNRS-Supélec-UPS), 3 rue Joliot-Curie, 91192 Gif-sur-Yvette France.*
+ *: EADS CCR, DCR/SP/PN, 12 rue Pasteur, 92152 Suresnes France.*

Abstract. In the framework of a collaborative project with EADS, a semi-analytical model based on a volume integral method has been developed to simulate eddy current (EC) inspection of riveted structures in aeronautics. The model handles a layered structure by considering a dyadic Green's approach where a fastener and a flaw are introduced as a variation of conductivity in a stack of slabs. Experimental data are used to validate the model.

Keywords. Eddy Current Testing, Aeronautic inspection

Introduction

EC technique is currently the operational tool used for fastener inspection which is an important issue for the maintenance of aircraft structures.The industry calls for faster, more sensitive and reliable NDT techniques for the detection and characterization of potential flaws nearby rivets. In order to reduce the development time, to optimize the design and to evaluate the performances of an inspection procedure, CEA and EADS have started a collaborative work aimed to extend the modelling features of the CIVA non destructive simulation platform to the simulation of multilayer assembly with fasteners. CIVA is a powerful multi-technique platform for industrial NDT (see [1], [2] and [3]). The developed EC simulation models are mainly based on the volume integral method using the dyadic Green's formalism detailed in [4]. Several examples of CIVA for eddy

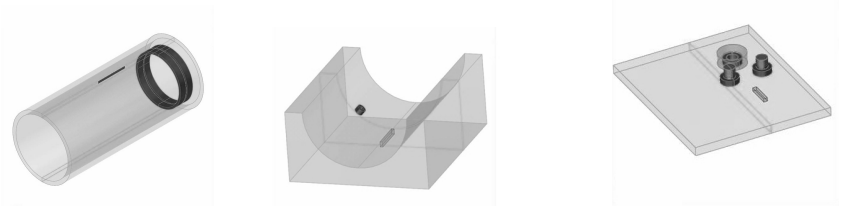

1.a: Bobbin coil placed inside a conducting tube

1.b: Bobbin coil placed on a configuration defined by CAD

1.c: Three ferrite cores placed on a conducting slab

Figure 1. Representation of several configurations affected by a parallelepiped flaw in the CIVA user interface

current testing are presented in Figure 1. This paper describes the progress in developing a 3D computer code for fastener modelling based on the volume integral equations which has the capability to quickly predict the response of an eddy current probe to 3D flaws.

1. Description of the model

1.1. Theoretical formulation

A typical configuration of interest is depicted in Figure 2. It consists of a layered planar structure with a fastener and a semi-elliptical flaw nearby the lower part of the rivet. The EC probe is moved along the surface, above the fastener assembly. This configuration

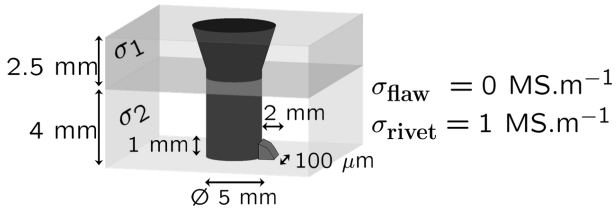

Figure 2. Typical aircraft configuration

can be attacked in two steps: (i) modelling the response of a probe to a layered structure with fastener without flaw; (ii) taking into account the flaw. Results of the first step are given below. Those of the second one are in progress and will be presented later. The configuration is described as follows: the space is divided in two air half-spaces numbered 0 and $N+1$ with, in between, a N-layer slab, each layer being numbered i and having a conductivity σ_i (all materials are supposed to be non magnetic and of air permeability μ_0). The slab is affected by a defect of volume Ω and conductivity $\sigma(\mathbf{r})$ crossing one or more layers (as depicted Figure 2). Let us denote with index m (resp. n) the first (resp. last) layer affected by the defect ($m < n$), the latter being sliced into as many layers as necessary such as $\Omega = \sum_{k=m}^{n} \Omega_k$ (note that, in the case of a rivet crossing the N layers without his foot, $m = 1$ and $n = N$). An exemple of the Ω domain for a two-layered slab is shown in Figure 3.a. A time-harmonic source (circular frequency ω and implied time-dependence $\exp(\mathrm{j}\omega t)$) –a coil probe for example– is placed in the upper half-space 0. The so-called vector domain integral formulation of the electric field $\mathbf{E}_k(\mathbf{r})$ in the layer k in such a configuration is obtained by application of the Green's theorem onto the diffusive vector wave equation and is given by

$$\mathbf{E}_k(\mathbf{r}) = \mathbf{E}_k^{(0)}(\mathbf{r}) - j\omega\mu_0 \sum_{l\,=\,m}^{n} \int_{\Omega_l} \overline{\overline{\mathbf{G}}}_{kl}^{(ee)}(\mathbf{r},\mathbf{r}')\,[\sigma_l - \sigma(\mathbf{r}')]\,\mathbf{E}_l(\mathbf{r}')\,d\mathbf{r}' \quad \forall \mathbf{r}' \in \Omega_k \tag{1}$$

where $\mathbf{E}_k^{(0)}(\mathbf{r})$ is the primary field in the layer k and $\overline{\overline{\mathbf{G}}}_{kl}^{(ee)}(\mathbf{r},\mathbf{r}')$ the electric-electric dyadic Green's functions defined as the field response for a unit point source and solution of

$$\nabla \times \nabla \times \overline{\overline{\mathbf{G}}}_{kl}^{(ee)}(\mathbf{r},\mathbf{r}') - k_k^2 \overline{\overline{\mathbf{G}}}_{kl}^{(ee)}(\mathbf{r},\mathbf{r}') = \delta_{kl}\overline{\overline{\mathbf{I}}}\delta(\mathbf{r}-\mathbf{r}'). \tag{2}$$

In the above equations k, l denote the index of the layer of the observation $\mathbf{r}$ and of the source $\mathbf{r}$' point, respectively, $\overline{\overline{\mathbf{I}}}$ is the unit dyadic and δ_{kl} stands for the Kronecker delta. k_l is the wave number in the l^{th} layer defined as $k_l^2 = \mathrm{j}\omega\mu_0\sigma_l$. The Green's dyad satisfies the appropriate boundary conditions at the interfaces between the different layers in the same way as the electric fields do. The response of the probe is given by its impedance variation is obtained via the reciprocity theorem, where I_0 is the feeding current of the probe, as

$$I_0^2 \Delta Z = \sum_{l\,=\,m}^{n} \int_{\Omega_l} \left[\sigma_l - \sigma(\mathbf{r})\right] \mathbf{E}_l^{(0)}(\mathbf{r}) \cdot \mathbf{E}_l(\mathbf{r}) d\mathbf{r}. \tag{3}$$

1.2. Numerical considerations

Once the model has been chosen and the equations established, the numerical formulation can be implemented. Equation (1) is discretized using a Galerkin's version of the method of moments where the contrast zone Ω is sliced in N_{cell} parallelepipeded voxels. The voxels are chosen in order to have an homogeneous conductivity inside each voxel, and in each voxel, the electric field is a constant-valued. This approach leads to a linear system (4)

$$\begin{bmatrix} \mathbf{E}_m^{(0)} \\ \vdots \\ \mathbf{E}_n^{(0)} \end{bmatrix} = \left(\mathbf{I} - \begin{bmatrix} \mathcal{G}_{m,m} \cdots \mathcal{G}_{m,n} \\ \vdots \quad \ddots \quad \vdots \\ \mathcal{G}_{n,m} \cdots \mathcal{G}_{n,n} \end{bmatrix} \right) \begin{bmatrix} \mathbf{E}_m \\ \vdots \\ \mathbf{E}_n \end{bmatrix} \tag{4}$$

where $\mathcal{G}_{i,i}$ are the electromagnetic self-coupling terms of the i^{th} region of the sliced rivet onto itself and where $\mathcal{G}_{i,j}$ are the mutual coupling terms of the j^{th} over the i^{th}.

An example is given for a two-layered slab ($n = 1$ and $m = 2$) in Figure 3. The rivet illustrated in Figure 3.a is here sliced into two parts, each one entirely contained in a single layer of conductivity σ_k with $k \in \{1, 2\}$. The self-coupling terms $\mathcal{G}_{i,i}$ with $i \in \{1, 2\}$ are represented in Figure 3.a and the mutual-coupling terms $\mathcal{G}_{i,j}$ with $(i, j) \in \{1, 2\}$ and $i \neq j$ are represented in Figure 3.b.

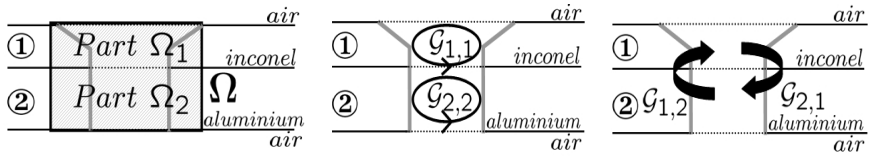

3.a: Rivet and the contrast zone Ω sliced in two inhomogeneous zones

3.a: Self-coupling

3.b: Mutual coupling

Figure 3. Example of a rivet in a two-layered slab

For building this multi-layer model, two main improvements have been made:

- Self-coupling terms: the planar stratification of the work piece is taken into account by introducing generalized reflection and transmission coefficients [4] at each interface in the Green's dyads.

- Mutual coupling terms: the mutual Green's functions are written in explicit analytical expressions [4] and implemented to reconstruct the entire matrix of equation (4).

In the applications we are interested in, the typical size of the domain Ω may be more than ten skin-depths which leads to a large number of voxels and to a too large linear system to invert (the memory size can be estimated as $\mathcal{O}\ (9\ N_{\text{cell}}^2)$). Taking into account the convolution structure of the integral equation (1) with respect to the two lateral directions via appropriate fast Fourier transforms, an iterative solution of the system allows us to treat larger defects by reducing the memory size to $\mathcal{O}\ (9\ N_{\text{cell}}^{4/3})$.

2. Validations

On one hand, the model is developed to handle a defined configuration –a rivet within a laminated slab– and from this point of view, we have to validate the two first aspects of the fastener modelling illustrated in Figure 4. On the other hand, this model is a multi-layer model –an inhomogeneous zone embedded in a laminated work piece– and therefore, we have to validate this multi-layer modelling also. In order to focus on these different aspects, and to avoid errors in rivet shape simulation, the rivet with its typical flat head shape is assumed in all validations to be a cylindrical through-wall hole. The flat head shape of the rivet can be obtained by introducing volume ratios in the calculation zone. Several validations have been done to improve the two approaches –handle a

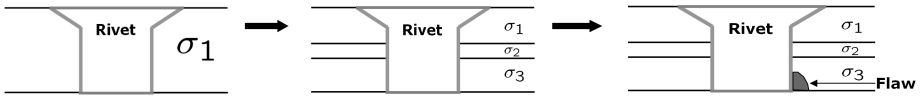

4.a: Rivet hole in one slab

4.b: Rivet crossing a multi-layer slab

4.c: Rivet in a multi-layer slab and a flaw nearby

Figure 4. Different aspects of fastener modelling

fastener in a laminated slab and a multi-layer configuration– of this multi-layer model:

- Fastener approach: through-wall inhomogeneous zone in one slab (first aspect, Figure 4.a) and in a two-layer slab (second aspect, Figure 4.b). The third aspect (Figure 4.c) is not treated here.
- Multi-layer approach: inhomogeneous zone contained successively in the different layers of a two-layer slab.

For all such studies, the same air-cored probe is used (an inner radius of 1 mm, an outer radius of 1.6 mm, a lift-off of 0.32 mm and a height of 2 mm with 320 turns) and is displaced along the diameter of the hole.

2.1. One-layer validation

An impedance meter HP4194 is used to measure the impedance of the air-cored probe working in absolute mode at the frequency of 10 kHz on a through-wall hole in an aluminium slab (Figure 5, left). The hole diameter is 4.9 mm and the slab thickness is 4 mm with a conductivity of 30 MS/m. The agreement between the model and the experimental data is better than 1% for the amplitude and 8° in phase (Figure 5, right).

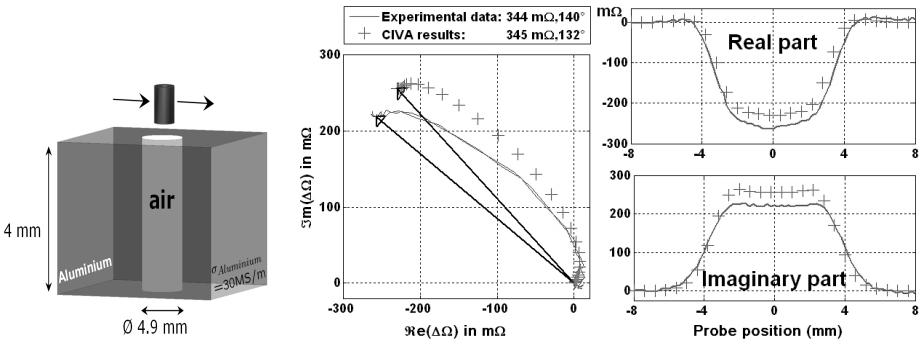

Figure 5. Cylindrical through-wall hole in one layer of aluminium (— experimental data, +++ CIVA results)

2.2. Multi-layer validations

The multi-layer modelling has been validated on a two-layer slab (mock-up inconel-aluminium) described as follows: an inconel slab with a conductivity of 1 MS/m and a thickness of 1.27 mm lies above an aluminium slab with a conductivity of 30 MS/m and a thickness of 4 mm. A cylindrical hole of 4.9 mm is crossing one (inconel slab, Figure 7.a) or the other (aluminium slab, Figure 8.a) or both (Figure 9.a). The air-cored probe is working here at 75 kHz.

2.2.1. Calibration

In most industrial applications, the measured EC signal is calibrated over a reference flaw. Preliminary to these validations, a calibration experiment has been made; the reference flaw is a surface breaking notch in an inconel slab with a conductivity of 1 MS/m. The EDM notch is 0.1 mm in width, 20 mm in length and 0.93 mm in depth and the thickness of the slab is 1.55 mm as shown in Figure 6 (left). The impedance variation measured in the impedance plane calibrated at 500 mV and 135° is presented in Figure 6 (right).

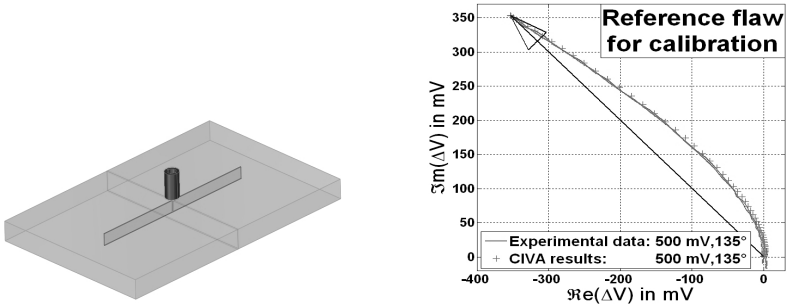

Figure 6. Response of the probe to a breaking notch in a slab (— experimental data, +++ CIVA results)

2.2.2. Imperfect matching slabs influence

For the hole in the inconel slab (like for the others but we will come back to them later on), the result is not completely satisfactory; even if the agreement for the measurement

of the EC signal in the impedance plane between the model and the experimental data is better than 4% for the amplitude and $2°$ in phase, the shapes of the signal are different (Figure 7.c). One of the reasons can be that the simulated configuration does not correspond exactly to the reality of the experimental configuration. As a matter of fact, in the experiment, the two slabs could not be fastened in perfect fashion (Figure 7.a, curve with ***), causing the occurrence of a thin air layer in between (Figure 7.b). A study has been carried out to evaluate the thickness of the layer of air to be taken into account and the best results have been obtained with a thickness of 50 µm (Figure 7.b). All the results presented in the next subsection take into account this air gap.

2.2.3. Results of validations

For the hole in the inconel slab, the agreement between the model and the experimental data is better than 6% for the amplitude and $2°$ in phase (Figure 7.c) whereas, for the hole in the aluminium slab, the agreement is better than 4% for the amplitude and $3°$ in phase (Figure 8.b). For the through-wall hole in the two-layer slab (Figure 9), the agreement between the model and the experimental data is better than 2% for the amplitude and $3°$ in phase (Figure 9.b).

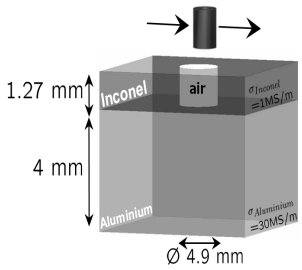

7.a: Cylindrical hole in the inconel layer with perfect matching

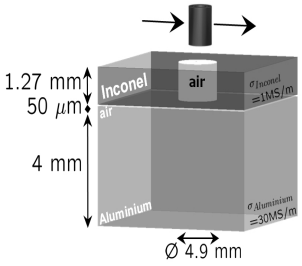

7.b: Cylindrical hole in the inconel layer with imperfect matching

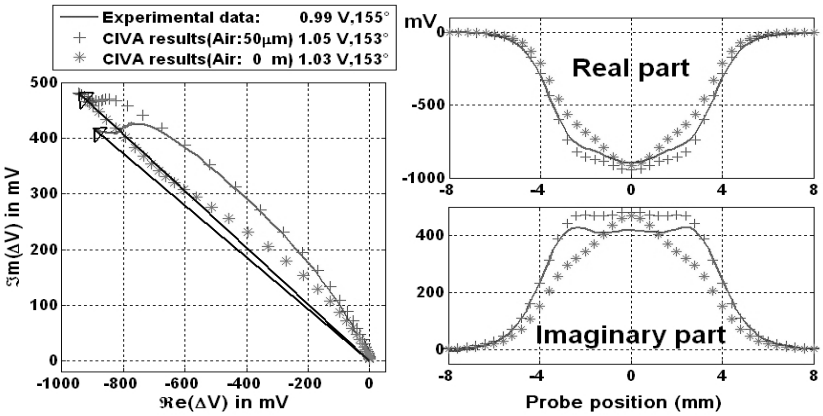

7.c: Calibrated signals in the impedance plane

Figure 7. Cylindrical hole in the inconel layer of a two-layer slab perfectly matched (— experimental data, *** CIVA results with perfect matching, +++ CIVA results with imperfect matching)

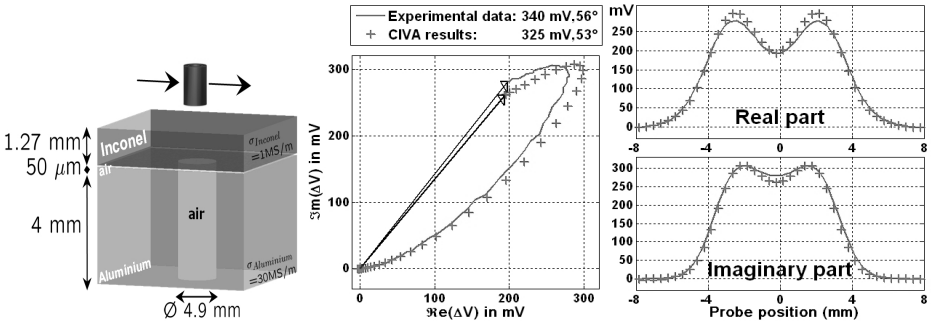

8.a: Hole in the aluminium layer with imperfect matching

8.b: Calibrated signals in the impedance plane with imperfect matching

Figure 8. Cylindrical hole in the aluminium layer of a two-layer slab (— experimental data, +++ CIVA results)

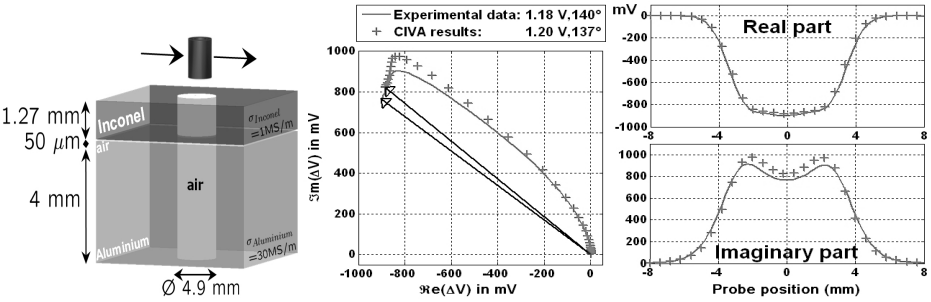

9.a: Hole crossing a two-layer slab with imperfect matching

9.b: Calibrated signals in the impedance plane with imperfect matching

Figure 9. Cylindrical through-wall hole in a two-layer slab (— experimental data, +++ CIVA results)

3. Application in aeronautics

Once the model has been validated, we can consider a realistic case: two identical multi-layered slabs held together by a rivet. We have applied the model to the calculation of the impedance variation of a ferrite-cored probe [1] used to test the aeronautical work piece illustrated in Figure 10. One slab is decomposed in three thin layers of aluminium alloy,

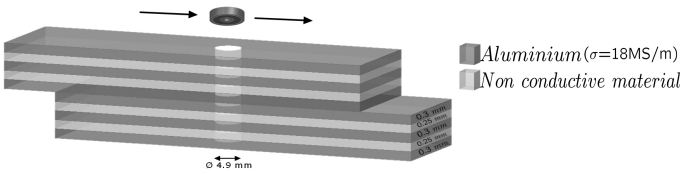

Figure 10. Cylindrical through-wall hole in two multi-layer slabs

bonded together with non-conductive material. The aluminium slabs are 0.3 mm in depth and the non-conductive slabs are 0.25 mm, the fastener hole has a diameter of 4.9 mm.

The cylindrical ferrite-cored probe used for these studies has an inner (resp. outer) radius of 3.74 mm (resp. 7.325 mm), and a height of 3.46 mm with 926 turns and works at 2.6 kHz. The results presented in Figure 11 have to be validated with experimental data,

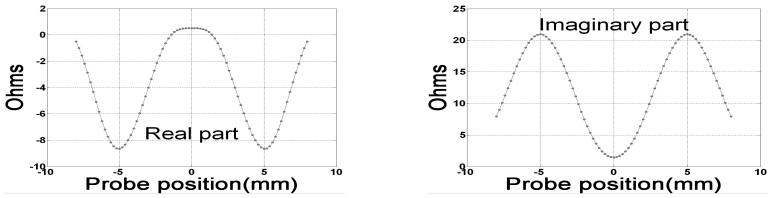

Figure 11. Simulated response of the probe to a cylindrical through-wall hole in two multi-layer slabs

however they are coherent with what is expected in such a configuration: (i) when the centre of the probe is exactly above the centre of the cylindrical hole, the signals are almost null because the inner diameter of the probe is larger than the diameter of the hole, and so the currents are almost undisturbed. (ii) when the centre of the probe is at 5 mm from the centre of the hole, the signals (Figure 11) are at their maximum (resp. minimum) for the real part (resp. for the imaginary part) corresponding to the positions where most of the winding is above the hole.

4. Conclusion and perspectives

The extension of the CIVA platform to the simulation of riveted structures is currently in progress. The multi-layer model is now validated, with a good agreement between the model and the experimental data, for a cylindrical through-wall hole in a set of two slabs, a cylindrical hole either in the top slab or in the bottom slab of the stack. A first milestone has been reached with the development of a model taking into account the presence of a rivet in a layered slab assembly. Validations with experimental data of the 3D model developed here for fastener modelling have been carried out successfully. Work is in progress to calculate the probe response due to the presence in a fastened structure of a rivet and an embedded flaw located nearby as shown in Figure 4.c.

Acknowledgements

This research is supported by the Paris Ile-de-France Region.

References

[1] Buvat F., Pichenot G., Prémel D., Lesselier D., Lambert M. and Voillaume H., *Eddy current modelling of ferrite-cored probes*, in Review of Progress in QNDE Vol. 24, 2005, pp. 463-470.

[2] Sollier T., Buvat F., Pichenot G. and Premel D., *Eddy current modelling of Ferrite-Cored Probes, application to the simulation of Eddy current signals from surface breaking flaws in austenitic steel*, Proc. 16th World Conf. on NDT, Montreal, 2004.

[3] Pichenot G., Buvat, F., Maillot V. and Voillaume H., *Eddy current modelling for non destructive testing*, Proc. 16th World Conf. on NDT, Montreal, 2004.

[4] Chew W.C., *Waves and Fields in Inhomogeneous Media*, Van Nostrand Reinhold, New York, 1990.